

DSC Study of SARS-CoV-2 ORF10 Protein and Its Complexes with Water-Soluble Metal Phthalocyanines

O. I. Koifman,^{a,b} S. S. Guseinov,^a N. Sh. Lebedeva,^a E. S. Yurina,^a M. O. Koifman,^{a,b} and Yu. A. Gubarev^{a@}

^aG.A. Krestov Institute of Solution Chemistry of the Russian Academy of Sciences, 153045 Ivanovo, Russia

^bIvanovo State University of Chemistry and Technology, 153000 Ivanovo, Russia

@Corresponding author E-mail: gua@isc-ras.ru

Dedicated to Academician Aslan Yu. Tsvadze on the occasion of his Anniversary

A theoretical and experimental study of the interaction of the SARS-CoV-2 ORF10 protein with sulfo-substituted cobalt(II) and copper(II) phthalocyanines was carried out. The structures of the most probable complexes of metal phthalocyanines with the ORF10 protein were obtained by molecular docking methods. Cobalt(II) tetrasulfophthalocyanine binds to the protein in the monomeric state, while the interaction of ORF10 with copper(II) tetrasulfophthalocyanine causes aggregation of the formed protein complexes, which was shown by the UV-Vis spectroscopy. Thermal denaturation of the ORF10 protein and its complexes with metal phthalocyanines was studied by differential scanning calorimetry. A joint analysis of the spectral and thermochemical data made it possible to propose a description of the mechanism of thermal denaturation of the ORF10 protein.

Keywords: SARS-CoV-2, protein, ORF10, phthalocyanine, DSC.

ДСК исследование белка ORF10 SARS-CoV-2 и его комплексов с водорастворимыми металлофталоцианинами

О. И. Койфман,^{a,b} С. С. Гусейнов,^a Н. Ш. Лебедева,^a Е. С. Юрина,^a М. О. Койфман,^{a,b} Ю. А. Губарев^{a@}

^aИнститут химии растворов им. Г.А. Крестова РАН, 153045 Иваново, Россия

^bИвановский государственный химико-технологический университет, 153000 Иваново, Россия

@E-mail: gua@isc-ras.ru

Проведено теоретическое и экспериментальное исследование взаимодействия дополнительного белка ORF10 SARS-CoV-2 с сульфозамещенными фталоцианинами кобальта(II) и меди(II). Методом молекулярного докинга получены структуры наиболее вероятных комплексов металлофталоцианинов с белком ORF10. Спектрально доказано, что тетрасульффталоцианин кобальта(II) связывается с белком в мономерной форме, в то время как взаимодействие ORF10 с тетрасульффталоцианином меди(II) вызывает агрегацию образующихся белковых комплексов. Методами дифференциальной сканирующей калориметрии изучены процессы термической денатурации белка ORF10 и его комплексов с металлофталоцианинами. Обобщение спектральных и термодинамических данных позволило предложить описание механизма термоденатурации белка ORF10.

Ключевые слова: SARS-CoV-2, белок, ORF10, фталоцианин, ДСК.

Introduction

In December 2019, the severe acute respiratory syndrome virus (SARS-CoV-2) has emerged in Wuhan, China, and triggered the global coronavirus pandemic (COVID-19).^[1,2] As of December 2022, more than 650 million cases

have been reported, with more than 6 million deaths. The virus is unusually contagious, with high fever, shortness of breath, dry cough, and can cause acute respiratory distress and, in some cases, cytokine storm.^[3-6]

SARS-CoV-2 is a positive-sense, single-stranded RNA virus that encodes 16 non-structural proteins (nsp1-

16) that serve to form the replicase mechanism of the virus.^[7,8] It also has four structural proteins, namely the spike (S), envelope (E), membrane (M), and nucleocapsid (N). In addition to structural and non-structural proteins, SARS-CoV-2 has seven accessory proteins (ORF3a, ORF3b, ORF6, ORF7a, ORF7b, ORF8, and ORF10) that modulate host responses to viral infections, thus promoting efficient infection and pathogenesis.^[9-11]

ORF10 is the smallest accessory protein (38 amino acid residues) of SARS-CoV-2, in early 2020 its presence was even questioned, since it had not previously been found in known coronaviruses.^[12] Later it was found that it is a unique protein and can be used to detect infection more reliably than PCR analysis.^[13] ORF10 is suitable for drug targeting because the genes encoding it are the most conserved (less susceptible to mutations).^[14] ORF10 contains a Molecular Recognition Function region (MoRF) in the first β -sheet, comprising amino acid residues 3 to 7 at the N-terminus.^[15] According to the authors, this is a protein interaction site that allows the ORF10 protein to adopt a set of conformations for binding to various proteins.^[16] Indeed, the presence of unstructured regions, two short beta chains and one hydrophobic alpha chain provides good conditions for binding ORF10 with a number of proteins. For example, ORF10 can interact with host proteins that are part of the Cullin-ubiquitin-ligase complex, which is required for viral pathogenesis.^[17-19] The paper^[20] reports that the partially disordered structure of SARS-CoV-2 ORF10 allows it to bind to the major histocompatibility complex, modulating the T-cell response. This is indirectly supported by the subcellular localization of ORF10, which may be located in the cytoplasm, but most of it is localized in the endoplasmic reticulum, which is important for interaction with the major histocompatibility complex.^[21] The ORF10 protein contains a large number of random epitopes of cytotoxic T-lymphocytes, primarily on the α -helix.^[20,22] Therefore, high levels of ORF10 expression can lead to an increased immune response and provoke a cytokine storm. It is believed that ORF10 affects the pathogenicity of the SARS-CoV-2 virus and has a multiple mechanism of action based on binding to other proteins.^[20,23-26] Obviously, it is important to search for compounds capable of inactivating this protein by preventing binding to other proteins due to shielding of a part of the ORF10 amino acid sequence or due to photo-damage of the protein catalyzed by photosensitizers. It is known that water-soluble metal phthalocyanines are capable of binding to proteins; as a rule, they can generate singlet oxygen in aqueous media; theoretically, they can be compounds capable of inactivating the viral ORF10 protein. Therefore, the purpose of this work was the spectral and thermochemical study of the ORF10 protein and its complexes with copper(II) and cobalt(II) tetrasulfophthalocyanines.

Experimental

Cobalt tetrasulfophthalocyanine was synthesized by the "urea fusion" method.^[27,28] The obtained melt was triturated, dissolved in water, the solution was filtered off, the filtrate was evaporated. The resulting substance was washed with concentrated hydrochloric acid to colorless filtrates and dried. The product was dissolved in water, the aqueous solution was passed through a column with a KU-2-8 cation exchange resin, and then chromatographed using silica gel and molselect G-10 successively as an

adsorbent, collecting the most colored zone. The resulting solution was evaporated, and the dry product was treated with organic solvents (methanol, acetone, benzene) in a Soxhlet apparatus. The product dried under vacuum at 100-110 °C. Elemental analysis found/calculated for $C_{32}N_8H_{16}S_4O_{12}Co$: C 42.5/43.1; H 1.9/1.8; N 12.3/12.6; S 14.2/14.4. UV-Vis (DMSO) λ_{max} nm (log ϵ): 664(5.15), 602(4.50), 330(4.85), which corresponds to the literature data.^[29] 1H NMR (D_2O) δ ppm: 10.02 b.s., 9.76 b.s., 8.68 b.s., 8.38 b.s., 8.09 m, 7.87 m.

The copper complex of sulfophthalocyanine was prepared in a similar manner. Elemental analysis found/calculated for $C_{32}N_8H_{16}S_4O_{12}Cu$: C 42.4/42.9; H 1.9/1.8; N 12.3/12.5; S 14.1/14.3. UV-Vis (DMSO) λ_{max} nm (log ϵ): 677 (5.41), 608 (4.59), 349 (4.75), which corresponds to the literature data.^[29] The purity of the tetrasulfophthalocyanines used in this work was no less than 98%.

ORF10 was expressed in *E. coli* BL21(DE3) cells based on pGBW-m4046950, which was a gift from Ginkgo Bioworks & Benjie Chen (Addgene plasmid 149258; <http://n2t.net/addgene:149258>; RRID: Addgene_149258). The procedure is described in detail in^[30].

Phosphate-buffered saline (PBS) was used for solution preparing. Double distilled water was used for solution preparing.

Molecular docking procedure. Structure of ORF10 predicted by D-I-Tasser (QHI42199.pdb) was downloaded from Zhang Lab website.^[31,32] The structures of the macroheterocyclic compounds (Figure 1) were minimized in the ORCA 4.0 program^[33] using the DFT method. Molecular docking of proteins with porphyrins was performed using AutoDock Vina 1.1.2^[34] and visualized with PyMol 2.4.1. The ligand and protein structure files were prepared using AutoDockTools 1.5.6. When preparing the structure of the ligand, rotating bonds were selected automatically. Polar hydrogens were added to the protein structure. The grid matrix was sized so that the protein molecule was completely overlapped. Due to the large size of the grid matrix, the exhaustiveness parameter was increased to 512.^[35] Molecular docking made it possible to find the 20 most favorable structures for each porphyrin. After analyzing the results, the most optimal positions indicated in Table 1 were selected. In the case of cationic and anionic macrocycles, the potential of the protein globule was additionally calculated by the ABPS method to analyze the docking sites.^[36]

UV-Vis spectra were registered using an AvaSpec-2048 spectrophotometer (Avantes BV, Netherlands), with a temperature-controlled cell at 25 °C.

Calorimetric experiments were carried out on a SCAL-1 differential scanning microcalorimeter (OOO Skal, Russia) with a glass cell with a volume of 0.337 ml at a scanning rate of 1.0 K/min, under a pressure of 2 atm. To obtain the values of the partial heat capacity of the protein, the SCAL program was used, based on the described algorithms.^[37,38] To obtain excess heat capacity curves, the heat capacities of the native and denatured states of the protein were linearly extrapolated to the region of the denaturation transition and subtracted from the values of the partial heat capacity of the protein using a "sigmoidal" baseline. For all calculations, the value for the partial volume of protein was assumed to be 0.73 cm³/g.

The calorimetric enthalpy ΔH_{cal} was determined as the area under the curve of excess heat capacity versus temperature. The Van't Hoff enthalpy (ΔH_{vH}) was determined from the calorimetric melting curve using the equation:

$$\Delta H_{vH} = 4RT_{max}^2 \cdot \Delta C_{P(max)} / \Delta H_{cal},$$

where R is the universal gas constant; T_{max} is the temperature corresponding to the maximum of the heat absorption curve; $\Delta C_{P(max)}$ is the value of excess heat capacity in T_{max} .

Results and Discussion

The method of molecular docking is widely used for the initial assessment of the possibility of binding biopoly-

mers with ligands, as well as for visualization of the resulting complexes. According to the simulation results, ORF10 forms stable complexes with the investigated sulfo-substituted metal phthalocyanines. Moreover, the binding energy is equal to 7.6 kcal/mol, as well as the localization in the protein is the same for the copper and cobalt complex of phthalocyanine with ORF10. According to the docking results (Figure 1), metal phthalocyanines bind to the hydrophobic region α -helix of the protein, forming hydrogen bonds between the sulfo groups of metal phthalocyanines with amino acid residues of the protein (Tyr26 (2.8Å), Met1(2.5Å), Asp31(2.4Å), Val32(2.4Å)).

Spectral studies of the interaction of ORF10 with metal phthalocyanines were carried out in PBS with $pH = 8$, since the isoelectric point of the protein is 8. CoPc in a buffer solution demonstrates two-band absorption with maxima at 628 and 667 nm, while CuPc in UV-Vis spectrum has a broad absorption band with a maximum at 619 nm and a shoulder in the region of 670 nm. Judging from the shape of the UV-Vis spectra, both metal phthalocyanines in PBS are dimerized, and in the case of the copper complex of phthalocyanine, the aggregation equilibrium is significantly shifted towards dimerization.

Titration of metal phthalocyanine solutions of ORF10 proteins causes significant changes in their UV-Vis spectra. In the case of CoPs, a shift of the aggregation equilibrium towards monomerization is recorded (Figure 2a) with a strong bathochromic shift of the Q band by 13 nm. The results obtained indicate that CoPc forms stable complexes with ORF10, in which CoPc is in the monomeric state. Such a strong bathochromic shift of the Q-band during complex formation indicates a change in the hydrate environment of the metal phthalocyanine to a pseudo-solvate, hydrophobic one, which is typical for protein α -helices. Thus, the experimental data confirm the results of molecular docking, according to which the docking of CoPc with ORF10 occurs in the region of α -helices.

An increase in the amount of the ORF10 protein in CuPc solutions has a different effect, namely, in the UV-Vis spectra of complexes, the optical density increases in the absorption region of dimers/associates, and a hypsochromic shift of the absorption maximum by 5 nm is recorded (Figure 2b). In addition, the light scattering of CuPc solutions with protein increases, compared with the individual protein at the same concentration. Probably, the interaction of CuPc with ORF10 leads to aggregation of the resulting protein complexes.

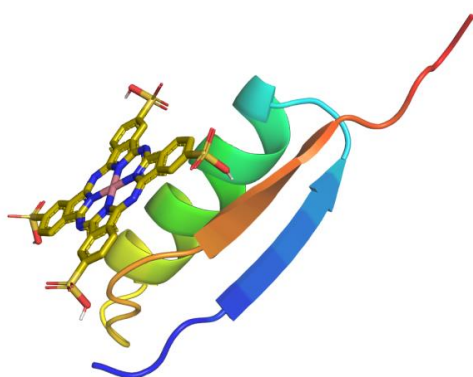


Figure 1. Results of molecular docking of ORF10 with CoPc.

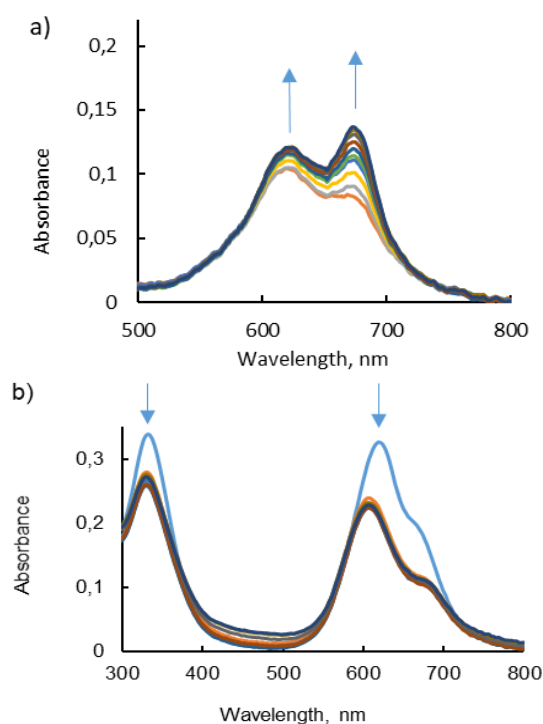


Figure 2. UV-Vis spectra of metallophthalocyanines upon titration by ORF10 protein in PBS: CoPc (a); CuPc (b).

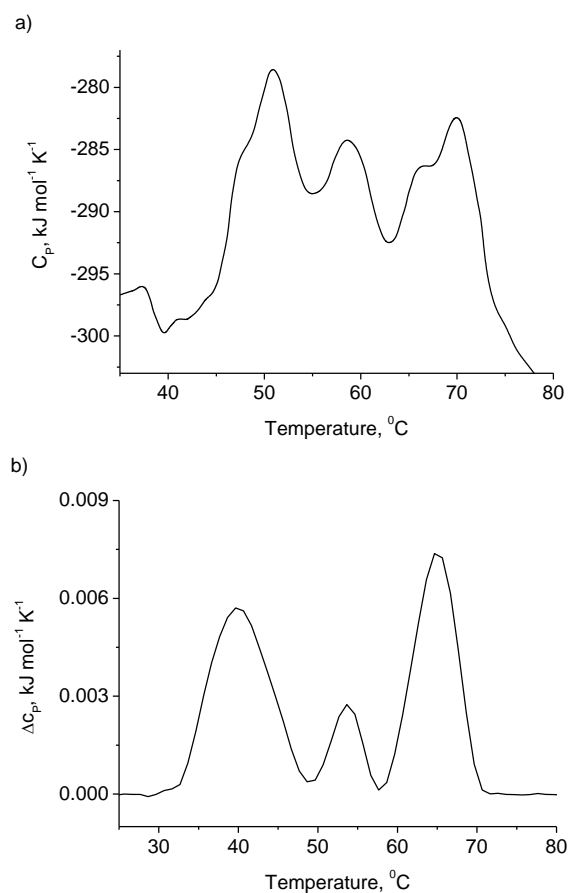


Figure 3. Temperature dependence of a) partial molar heat capacity of the ORF10 protein; b) excess molar heat capacity of the ORF10 protein.

Valuable information about the effect of complex formation of MHC with proteins on protein properties and its thermochemical behavior can be obtained by differential scanning calorimetry. The calorimetric curve of the temperature dependence of the partial molar heat capacity of the ORF10 protein, shown in Figure 3a, has a rather complex form. Three endothermic effects are observed in the studied temperature range. As a rule, small and medium-sized proteins unfold in a single cooperative step, which is reflected in the thermogram as a simple uniform peak. In this case, although ORF10 belongs to small proteins, its denaturation is stepwise; when ORF10 is heated, various events occur, it can be partial denaturation of one of the protein fragments, aggregation, *etc.*

The partial molar heat capacity of proteins, as is known, varies over the entire temperature range, while there are two fundamentally different temperature regions. The region where there are no cooperative conformational rearrangements covering large areas of the molecule, and, in fact, the region of the denaturation transition. Assuming that pre- and post-denaturation heat capacities are linear functions of temperature, and therefore extrapolating the heat capacity of the native and denatured states to the entire temperature range under study, the temperature dependence of the excess molar heat capacity of ORF10 was obtained (Figure 3b). As can be seen (Figure 3b), the change in the excess molar heat capacity (ΔC_p) of ORF10 is positive. When heated, the protein denatures, and its hydrophobic regions, which in the native conformational state of the protein are oriented inside the globule, appear on its surface. The positive change in ΔC_p of the ORF10 protein is due to the relatively high heat capacity C_p of water molecules around the side chains of nonpolar amino acids that appeared on the surface of the globule when the protein was heated.

This conclusion is consistent with generally accepted data^[39] that the main processes that require a significant amount of energy during protein denaturation are additional hydration of the surface of the protein molecule, previously hidden in the structure of the folded globule, and disruption of internal interactions. The heat capacity of proteins in the native state is determined mainly by the nature of the surface of the native structure, accessible to the solvent. The entropy of denaturation is mainly determined by two contributions, namely, the entropy resulting from additional hydration and the change in the configurational entropy of the molecule due to the release of the backbone and rotation of the side groups.^[40]

The temperature dependence of ΔC_p of the ORF10 protein, shown in Figure 3b, consists of three overlapping peaks with temperatures equal to 39.9, 53.8 and 65.1 °C. Calorimetric enthalpies of denaturation ($\Delta_{cal}H$) calculated as areas under each peak, van't Hoff effective enthalpies

$\Delta_{v-H}H$ and activation energies of denaturation ΔE_a are shown in Table 1.

It should be noted that the calorimetric enthalpies are small and probably characterize the low-energy transition processes that occur in the ORF10 protein upon heating. As can be seen from Table 1, $\Delta_{cal}H$ of the first and third peaks are equal and significantly higher than for the second peak, while the effective van't Hoff enthalpy and activation energy ORF10 for the second process, on the contrary, are higher than for the first and third peaks. The van't Hoff criterion $\Delta_{cal}H/\Delta_{v-H}H$ for all three stages is significantly below unity, which indicates that the protein molecule is melting in parts. Analyzing the data in Table 1 and Figure 3, two possible models of reversible unfolding and subsequent irreversible denaturation of ORF10 were suggested.

According to the first model, a partial reversible unfolding of the protein occurs at the first stage. By analogy with other proteins, it can be assumed that the part of the protein undergoing melting is α -helical regions. At the same stage, energy is required to destroy the hydration shell of the macromolecule, which prevents the unfolding process. Then a partial low-energy aggregation of the protein occurs with a change in the structure of the hydration shell. With a further increase in temperature, aggregates are destroyed, followed by irreversible denaturation of the protein at the last stage (peak 3). However, the van't Hoff criterion at the third stage is 0.133, while it should be greater than 1 upon melting of aggregates. Therefore, we also considered an alternative denaturation model. According to it, at the first stage, a reversible unfolding of the protein occurs with a change in the structure of the hydration shell (partial dehydration). Solvent molecules penetrate into the cavities formed during protein unfolding, interact with protein domains, and prevent further unfolding. In the scientific literature, such a phenomenon is described by the term "molten globule", *i.e.* the globular structure is preserved, but the protein is saturated with solvent molecules. Subsequent heating of the solution leads to a weakening of the interaction of the solvent with the amino acid residues lining the protein cavities, which in turn probably leads to changes in the environment of the entire protein. In other words, structural changes around the protein (entropy factor) contribute to the further unfolding process, which is already irreversible.

It is interesting to note that the UV-Vis spectra of the ORF10 protein change in different temperature ranges of 35-55, 55-70 and 75-90 °C. Each specified interval has its own isosbestic point: 35-55 °C at 300 nm, 55-70 °C at 245 nm and 75-90 °C at 265 nm. Analyzing the obtained thermal profiles of the protein, taking into account three isosbestic points, it can be assumed that the three endothermic effects observed on DSC correspond to thermally induced processes associated with changes in the secondary and tertiary structure of the protein.

Table 1. Thermodynamic parameters of thermal denaturation of ORF10.

	$T_{max}, ^\circ C$	$\Delta C_{P(max)}, kJ \cdot mol^{-1} \cdot K^{-1}$	$\Delta_{cal}H, kJ \cdot mol^{-1}$	$\Delta_{v-H}H, kJ \cdot mol^{-1}$	$\Delta_{cal}H/\Delta_{v-H}H$	$E_a, kJ \cdot mol^{-1}$
Peak 1	39.9	13.3	85	547	0.155	372
Peak 2	53.8	5.5	22	899	0.025	611
Peak 3	65.1	13.9	85	641	0.133	435

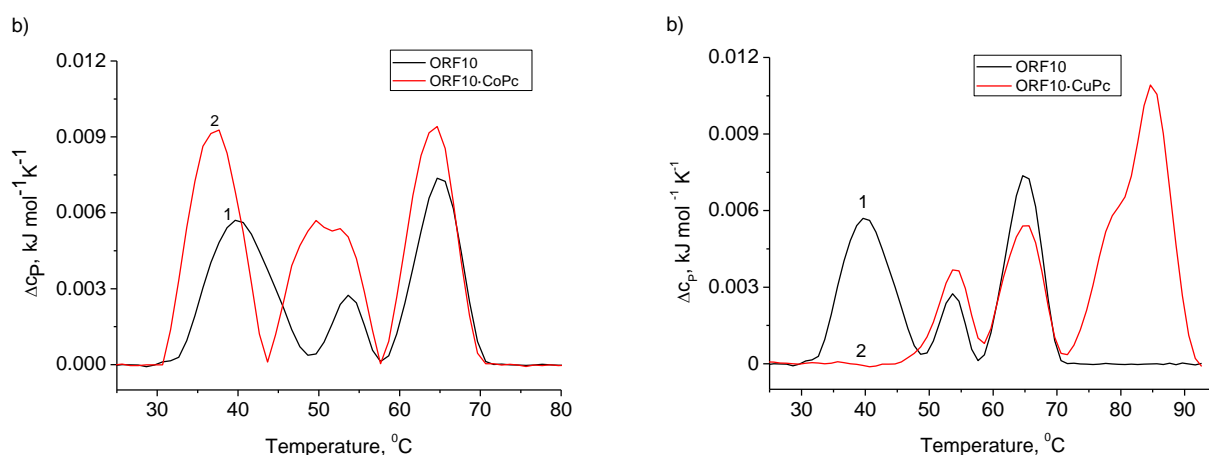


Figure 4. Temperature dependences of the excess molar heat capacity (ΔC_p) of solutions: a) ORF10 (line 1), ORF10+CoPc (line 2); b) ORF10 (line 1) and ORF10+CuPc (line 2).

Table 2. Temperature characteristics of thermally induced denaturation of the ORF10 protein and its complexes with sulfo-substituted metal phthalocyanines.

	T_{start1}	T_{max1}	T_{end1}	T_{start2}	T_{max2}	T_{end2}	T_{start3}	T_{max3}	T_{end3}
ORF10	32.3	39.8	48.9	49.5	53.7	57.7	58.1	64.9	72.1
ORF10-CoPc	30.7	37.8	43.7	44.0	49.8 (52.5 shoulder)	57.7	58.0	64.7	71.7
ORF10-CuPc	45.0	54.2	58.0	58.7	65.2	70.7	71.6	84.9 (shoulder 80.0)	92.8

As an example, Figure 4 shows the temperature dependences of the excess molar heat capacities of the ORF10 protein and its complexes with metal phthalocyanines. The temperature characteristics of the start, maxima and end of the processes characterizing the stages of denaturation of the ORF10 protein and complexes with CoPc and CuPc are given in Table 2.

For all the studied solutions, three consecutive endothermic peaks passing one into another are observed, but the thermal effects and temperatures of these transitions are different. In the case of ORF10 with CoPs, complexation leads to a decrease in the temperature at the start of the first two steps. Probably, relatively small changes in the temperature intervals of three transitions between two states for the analyzed solutions indicate the same type of processes, but at the same time, different energies of interaction between the polypeptide chains of the protein in the free form and the complex, and for this reason, different contributions of the entropy factor. This is an important point, since if the process of ORF10 denaturation was carried out according to the first model, then the first stage associated with a change in the conformation of the α -helix would change significantly, due to the fact that CoPc binds precisely to the α -helix. Judging by the data obtained (Figure 4a), this does not happen, therefore, the proposed model of ORF10 denaturation through the "molten globule" stage is more likely. According to the data presented in Figure 4a and Table 2, the temperatures of the third transition for ORF10 and its complex with CoPc coincide within the error. Obviously, the final state of all the studied systems does not depend on the previous structural changes in solutions.

In the case of the complex of ORF10 protein with CuPc, the temperatures of each of the three transitions are significantly higher than those for the protein and the complex of the protein with CoPc. According to the data given in Table 2, the transition temperature differences (peak maxima) between the states are approximately 17, 15 and 20 °C, respectively. It is possible that the reason for protein stabilization is associated with aggregation processes caused by CuPc upon interaction with ORF10. The results obtained indicate significant changes in the mechanism of protein denaturation.

Based on the results of theoretical and experimental studies of the processes of interaction of the SARS-CoV-2 additional ORF10 protein with sulfo-substituted copper(II) and cobalt(II) phthalocyanines, it can be concluded that the use of the cobalt complex of metal phthalocyanine is more preferable for inactivation of the hydrophobic part of the protein.

Conclusions

A spectral and thermochemical study of the additional SARS-CoV-2 ORF10 protein and its complexes with sulfo-substituted cobalt(II) and copper(II) phthalocyanines was carried out. It has been established that the ORF10 protein undergoes thermal denaturation; this process is multistage. The most probable mechanism of denaturation of the ORF10 protein was proposed, which includes the stage of obtaining a "molten globule". It was found that in buffer solutions $pH=8$, the ORF10 protein forms complexes with the CoPc monomer, shifting the dimer-monomer phthalocyanine

cyanine aggregation equilibrium towards monomerization. Complexation of ORF10 with CoPc slightly reduces the resistance of the protein to thermally induced denaturation, while maintaining the mechanism as a whole. The interaction of the ORF10 protein with CuPc leads to the aggregation of protein complexes with metal phthalocyanine. Aggregates of ORF10 with CuPc are more thermally stable, and the process of their denaturation proceeds according to a different mechanism, which differs significantly from the mechanism of denaturation of ORF10 and its complex with CoPc.

Acknowledgements. This work was financially supported by the Russian Science Foundation (grant no. 21-73-20140). We are grateful to the center "The upper Volga region centre of physico-chemical research" for analysis of the investigated samples.

References

- Ciotti M., Ciccozzi M., Terrinoni A., Jiang W.-C., Wang C.-B., Bernardini S. *Crit. Rev. Clin. Lab. Sci.* **2020**, *57*, 365. DOI: 10.1080/10408363.2020.1783198.
- Wu F., Zhao S., Yu B., Chen Y.-M., Wang W., Song Z.-G., Hu Y., Tao Z.-W., Tian J.-H., Pei Y.-Y. *Nature* **2020**, *579*, 265. DOI: 10.1038/s41586-020-2008-3.
- Rai B., Shukla A., Dwivedi L.K. *J. Public Health* **2022**, *30*, 2649. DOI: 10.1007/s10389-021-01478-1.
- Huang C., Wang Y., Li X., Ren L., Zhao J., Hu Y., Zhang L., Fan G., Xu J., Gu X. *Lancet* **2020**, *395*, 497. DOI: 10.1016/S0140-6736(20)30183-5.
- Hu B., Huang S., Yin L. *J. Med. Virol.* **2021**, *93*, 250. DOI: 10.1002/jmv.26232.
- Mehta P., McAuley D.F., Brown M., Sanchez E., Tattersall R.S., Manson J.J. *Lancet* **2020**, *395*, 1033. DOI: 10.1016/S0140-6736(20)30628-0.
- Kim D., Lee J.-Y., Yang J.-S., Kim J. W., Kim V. N., Chang H. *Cell* **2020**, *181*, 914. DOI: 10.1016/j.cell.2020.04.011.
- Michel C.J., Mayer C., Poch O., Thompson J. D. *Virol. J.* **2020**, *17*, 1. DOI: 10.1186/s12985-020-01402-1.
- Haque S. M., Ashwaq O., Sarief A., Azad John Mohamed A. K. *Future Virol.* **2020**, *15*, 625. DOI: 10.2217/fvl-2020-0124.
- Yan R., Zhang Y., Li Y., Xia L., Guo Y., Zhou Q. *Science* **2021**, *367*, 1444. DOI: 10.1126/science.abb2762.
- Shang J., Ye G., Shi K., Wan Y., Luo C., Aihara H., Geng Q., Auerbach A., Li F. *Nature* **2020**, *581*, 221. DOI: 10.1038/s41586-020-2179-y.
- Pancer K., Milewska A., Owczarek K., Dabrowska A., Kowalski M., Labaj P. P., Branicki W., Sanak M., Pyrc K. *PLoS Path.* **2020**, *16*, e1008959. DOI: 10.1371/journal.ppat.1008959.
- Koyama T., Platt D., Parida L. *Bull. W.H.O.* **2020**, *98*, 495. DOI: 10.2471/BLT.20.253591.
- Shah A., Rehmat S., Aslam I., Suleman M., Batool F., Aziz A., Rashid F., Nawaz M. A., Ali S.S., Junaid M. *Comput. Biol. Med.* **2022**, *141*, 105170. DOI: 10.1016/j.compbiomed.2021.105170.
- Giri R., Bhardwaj T., Shegane M., Gehi B. R., Kumar P., Gadhve K., Oldfield C. J., Uversky V. N. *Cell. Mol. Life Sci.* **2021**, *78*, 1655. DOI: 10.1007/s00018-020-03603-x.
- Uversky V. N. *Chem. Soc. Rev.* **2011**, *40*, 1623. DOI: 10.1039/C0CS00057D.
- Mahon C., Krogan N. J., Craik C. S., Pick E. *Biomolecules* **2014**, *4*, 897. DOI: 10.3390/biom4040897.
- Gordon D. E., Jang G. M., Bouhaddou M., Xu J., Obernier K., White K. M., O'Meara M. J., Rezelj V. V., Guo J. Z., Swaney D. L. *Nature* **2020**, *583*, 459. DOI: 10.1038/s41586-020-2286-9.
- Li J., Guo M., Tian X., Wang X., Yang X., Wu P., Liu C., Xiao Z., Qu Y., Yin Y. *Med* **2021**, *2*, 99. DOI: 10.1016/j.medj.2020.07.002.
- Hassan S.S., Attrish D., Ghosh S., Choudhury P.P., Uversky V.N., Aljabali A.A., Lundstrom K., Uhal B.D., Rezaei N., Seyran M. *Int. J. Biol. Macromol.* **2021**, *181*, 801. DOI: 10.1016/j.ijbiomac.2021.03.199.
- Zhang J., Cruz-Cosme R., Zhuang M.-W., Liu D., Liu Y., Teng S., Wang P.-H., Tang Q. *Sig. Transduct. Target Ther.* **2020**, *5*, 269. DOI: 10.1038/s41392-020-00372-8.
- Mishra S. *R. Soc. Open Sci.* **2020**, *7*, 201141. DOI: 10.1098/rsos.201141.
- Corman V.M., Ithete N.L., Richards L.R., Schoeman M.C., Preiser W., Drosten C., Drexler J.F. *J. Virol.* **2014**, *88*, 11297. DOI: 10.1128/JVI.01498-14.
- Hui D.S., Azhar E.I., Madani T.A., Ntoumi F., Kock R., Dar O., Ippolito G., Mchugh T.D., Memish Z.A., Drosten C. *Int. J. Infect. Dis.* **2020**, *91*, 264. DOI: 10.1016/j.ijid.2020.01.009.
- Yang W., Kandula S., Huynh M., Greene S.K., Van Wye G., Li W., Chan H.T., McGibbon E., Yeung A., Olson D. *Lancet Infect. Dis.* **2021**, *21*, 203. DOI: 10.1016/S1473-3099(20)30769-6.
- Hassan S.S., Choudhury P.P., Dayhoff II G.W., Aljabali A.A., Uhal B.D., Lundstrom K., Rezaei N., Pizzol D., Adadi P., Lal A. *Arch. Biochem. Biophys.* **2022**, *717*, 109124. DOI: 10.1016/j.abb.2022.109124.
- Weber J.H., Busch D.H. *Inorg. Chem.* **1965**, *4*, 469. DOI: 10.1021/ic50026a007.
- Shaposhnikov G., Kulinich V., Maizlish V. *Modified Phthalocyanines and Their Structural Analogs*. Moscow: Krasand, **2012** [Шапошников Г.П., Кулинич В.П., Майзлиш В.Е. Модифицированные фталоцианины и их структурные аналоги. М.: Красанд, **2012**. 480 с.].
- Maizlish V., Mochalova N., Snegireva F., Borodkin V. *ChemChemTech [Izv. Vyssh. Uchebn. Zaved. Khim. Khim. Tekhnol.]* **1986**, *29*(1), 3.
- Koifman M., Malyasova A., Romanenko Y.V., Yurina E., Lebedeva N.S., Gubarev Y.A., Koifman O. *Spectrochim. Acta, A* **2022**, *279*, 121403. DOI: 10.1016/j.saa.2022.121403.
- Zhang C., Zheng W., Huang X., Bell E.W., Zhou X., Zhang Y. *J. Proteome Res.* **2020**, *19*, 1351. DOI: 10.1021/acs.jproteome.0c00129.
- Zheng W., Zhang C., Li Y., Pearce R., Bell E.W., Zhang Y. *Cell Reports Methods* **2021**, *100014*. DOI: 10.1016/j.crmeth.2021.100014.
- Neese F. *WIREs Comput. Mol. Sci.* **2022**, *12*, e1606. DOI: 10.1002/wcms.1606.
- Trott O., Olson A.J. *J. Comput. Chem.* **2010**, *31*, 455. DOI: 10.1002/jcc.21334.
- Rentzsch R., Renard B.Y. *Brief. Bioinform.* **2015**, *16*, 1045. DOI: 10.1093/bib/bbv008.
- Baker N.A., Sept D., Joseph S., Holst M.J., McCammon J.A. *Proc. Natl. Acad. Sci. U.S.A.* **2001**, *98*, 10037. DOI: 10.1073/pnas.181342398.
- Senin A., Potekhin S., Tiktopulo E., Filomonov V. *J. Therm. Anal. Calorim.* **2000**, *62*, 153. DOI: 10.1023/A:1010171013669.
- Privalov P.L. *Adv. Protein Chem.* **1979**, *33*, 167. DOI: 10.1016/S0065-3233(08)60460-X.
- Falconer R.J. *Differential Scanning Calorimetry and Related Techniques*. In: *Encyclopedia of Biophysics* (Roberts G., Watts A., Eds.). Springer, Berlin, Heidelberg, **2018**. DOI: 10.1007/978-3-642-35943-9_10062-1.
- Potekhin S.A. *Transition States and Domain Organization of Proteins*, Diss. doc. phys.-math. sci., "Biophysics" Pushchino, **1999**.

Received 13.12.2022

Accepted 11.02.2023